

Soliton Wall Superlattice Charge-Density-Wave Phase in Quasi-One-Dimensional Conductor $(\text{Per})_2\text{Pt}(\text{mnt})_2$

Si Wu and A.G. Lebed*

*Department of Physics, University of Arizona,
1118 E. 4th St., Tucson, AZ 85721*

(Dated: March 24, 2009)

Abstract

We demonstrate that the Pauli spin-splitting effects in a magnetic field improve nesting properties of a realistic quasi-one-dimensional electron spectrum. As a result, a high resistance Peierls charge-density-wave (CDW) phase is stabilized in high enough magnetic fields in $(\text{Per})_2\text{Pt}(\text{mnt})_2$ conductor. We show that, in low and very high magnetic fields, the Pauli spin-splitting effects lead to a stabilization of a soliton wall superlattice (SWS) CDW phase, which is characterized by periodically arranged soliton and anti-soliton walls. We suggest experimental studies of the predicted first order phase transitions between the Peierls and SWS phases to discover a unique SWS phase. It is important that, in the absence of a magnetic field and in a limit of very high magnetic fields, the suggested model is equivalent to the exactly solvable model of Brazovskii, Dzyaloshinskii, and Kirova.

PACS numbers: 71.45.Lr, 74.70.Kn, 71.10.-w

I. INTRODUCTION

It is well known that the charge-density-wave (CDW) phases are generally destroyed by a magnetic field due to the Pauli spin-splitting effects, i.e., they are paramagnetically limited^{1–6}. On the other hand, the spin-density-wave (SDW) phases are not sensitive to the Pauli spin-splitting effects^{2,7–12}. In some quasi-one-dimensional (Q1D) organic materials, the field induced dimensional crossovers in an electron motion^{2,7} can even enhance the SDW instability and lead to a cascade of phase transitions, which is known as the field-induced spin-density-wave (FISDW) one^{2,7–12}. This idea has been also applied to the CDW phases^{3,4}, where the field induced dimensional crossovers are shown to restore the CDW instability, but only at rather low temperatures⁴. Therefore, the recent discovery of a high resistance state in Q1D materials $(\text{Per})_2\text{X}(\text{mnt})_2$ ($\text{X} = \text{Pt}$ and Au) at high magnetic field by Graf *et al*¹³ is very surprising and interesting.

Originally, the above mentioned phenomenon is explained^{13–15} in terms of the dimensional crossovers effects^{2–4,7}. This explanation may work for $(\text{Per})_2\text{Au}(\text{mnt})_2$, where the high resistance state is observed only for a magnetic field, applied perpendicular to the conducting planes, $\mathbf{H} \parallel \mathbf{c}$, and, thus, the orbital effects play an important role. In a sister compound $(\text{Per})_2\text{Pt}(\text{mnt})_2$, however, the high resistance state is observed at any direction of a magnetic field^{13,14}. In particular, when magnetic field is parallel to the conducting chains, $\mathbf{H} \parallel \mathbf{b}$, the dimensional crossovers effects^{2–4,7} do not occur. Therefore, the observations of the high resistance state in $(\text{Per})_2\text{Pt}(\text{mnt})_2$,^{13,14} which is almost independent on a direction of a magnetic field, indicates that this unique phenomenon cannot be explained by the previous theories^{1–4,7–10}.

Based on the band calculation¹⁶ and the experiments^{17,18}, we have proposed a simplified but realistic Q1D model electron spectrum to explain the main features of the phase diagram in $(\text{Per})_2\text{Pt}(\text{mnt})_2$ conductor¹⁹. We have demonstrated that the Pauli spin-splitting effects improve nesting conditions for the suggested Fermi surface and, therefore, a traditional Peierls CDW state restores at high magnetic fields. We have also suggested a hypothesis¹⁹ that, at low and higher enough magnetic fields, a unique soliton wall superlattice (SWS) phase may appear. This phase is characterized by two gaps in the corresponding electron spectrum and by periodically arranged soliton and anti-soliton walls in a real space. The distance between these walls and values of the gaps in an energy spectrum depend on a value

of a magnetic field. Below, we study the phase diagram in more details. The main result of the present paper is a confirmation of the above mentioned hypothesis¹⁹. In particular, we calculated the Landau free energy, minimize it, and show that, indeed, the SWS phase is a ground state at low and high enough magnetic fields. We also demonstrate that the phase transitions between the Peierls and SWS phases are of the first order and suggest some experimental methods to discover the unique SWS phase.

The outline of the paper is as follows. In Sec. II, the spin improved nesting phenomenon, which is crucial for understanding of the phase diagram in $(\text{Per})_2\text{Pt}(\text{mnt})_2$ conductor, is discussed qualitatively. Then, a transition line from metallic phase to the CDW phase is determined in Sec. III by means of finite temperature Green functions technique. In Sec. IV, a free energy relative to a metallic phase is calculated, which allows to obtain a detailed phase diagram.

II. SPIN IMPROVED NESTING

To begin with, let us discuss the spin improved nesting phenomenon, which results in a stabilization of the traditional Peierls CDW state at high enough magnetic fields in $(\text{Per})_2\text{Pt}(\text{mnt})_2$ conductor. We use the following simplified model electron spectrum, corresponding to four plane sheets of the Fermi surface,

$$\varepsilon_{\alpha}^{\pm}(\mathbf{p}) = \pm v_F [p_y \mp p_F \pm (\Delta p/2)(-1)^{\alpha}]. \quad (1)$$

[Here p_F and v_F are the average Fermi momentum and the Fermi velocity, $+(-)$ stands for right (left) part of the Fermi surface, $\alpha = 1(2)$ stands for the first (second) conducting perylene chain, Δp is a difference between values of the Fermi momenta on two different conducting chains, and p_y is an electron momentum along the conducting direction.] Note that this model is based on numerical band calculations¹⁶ and experimentally observed quantum interference oscillations¹⁷ and Landau level quantization¹⁸. Although the band calculations¹⁶ indicate that the actual Fermi surface consists of eight slightly corrugated open sheets, four of them are almost identical to the other four, and, thus, we do not distinguish between them. Notice that in Eq.(1) we also ignore electron motion in perpendicular to the chains directions. This seems to be legitimate in $(\text{Per})_2\text{Pt}(\text{mnt})_2$ since the corrugations of the open sheets of the Fermi surface (1) are less than the distance between the Fermi

surfaces, Δp .^{16,17}

In a magnetic field, the electron spectrum (1) is split into eight sheets,

$$\varepsilon_{\alpha\sigma}^{\pm}(\mathbf{p}) = \pm v_F[p_y \mp p_F \pm (\Delta p/2)(-1)^{\alpha}] - \sigma\mu_B H, \quad (2)$$

where $\sigma = \pm 1$ is a spin component of the electron along a direction of a magnetic field and μ_B is the Bohr magneton. As shown in Fig.1, there exist four different nesting vectors competing with each other, $Q_{1,+1}$, $Q_{1,-1}$, $Q_{2,+1}$, and $Q_{2,-1}$. Note that the Peierls CDW instability, which results from pairing of electrons and holes with the same spins and with momenta difference $2p_F$, is, thus, paramagnetically limited. This is clearly seen from Fig.1. Indeed, two original nesting vectors,

$$Q = 2p_F \pm \Delta p, \quad (3)$$

are split in the presence of a magnetic field into four ones,

$$Q_{\alpha\sigma} = 2p_F + q_{\alpha\sigma}, \quad q_{\alpha\sigma} = (-1)^{\alpha}\Delta p - 2\sigma\mu_B H/v_F, \quad (4)$$

which decreases instability to a formation of the CDW. Moreover, the existence of these four nesting vectors may even correspond to the appearance of several energy gaps in an electron spectrum at high values of the parameters Δp and $2\mu_B H/v_F$. Our theoretical results, as shown below, confirm the appearance of the SWS phase with two energy gaps, which is in a qualitative agreement with a general theory of solitons and soliton superstructures^{20–24}.

However, according to Fig.1 and Eq. (4), at some critical value of a magnetic field,

$$H_p^* = \Delta p v_F / 2\mu_B, \quad (5)$$

two of the nesting vectors coincide, $Q_{1,-1} = Q_{2,+1} = 2p_F$, and the number of nesting vectors decreases to three, which improves the nesting conditions. Moreover, according to Eq. (4), a half of the original sheets of Fermi surface are nested with $Q = 2p_F$. Therefore, we expect a restoration of the traditional Peierls CDW phase with one gap in an electron spectrum in the vicinity of $H \approx H_p^*$ (see Figs. 2, 3). These statements are confirmed later by our theoretical analysis.

III. METAL-CDW TRANSITION LINE

Now let us consider the CDW phase with nesting vector,

$$\mathbf{Q} = (0, 2p_F + q, 0), \quad (6)$$

and the CDW order parameter,

$$\Delta_{CDW}(x) = \Delta_q e^{i(2p_F+q)x} + \Delta_q^* e^{-i(2p_F+q)x}. \quad (7)$$

Below, we use the finite temperature Green function method²⁵ to study the metal-CDW phase transition line. We consider the following standard mean field Hamiltonian,

$$\begin{aligned} \hat{H} = & \sum_{\alpha=1,2} \sum_{\sigma=\pm 1} \sum_{\xi} \left\{ a_{\alpha\sigma}^{\dagger}(\xi) a_{\alpha\sigma}(\xi) [\varepsilon_{\alpha\sigma}^+(\xi) - \mu] + b_{\alpha\sigma}^{\dagger}(\xi) b_{\alpha\sigma}(\xi) [\varepsilon_{\alpha\sigma}^-(\xi) - \mu] \right\} \\ & + \sum_{\alpha=1,2} \sum_{\sigma=\pm 1} \sum_{\xi} \left\{ a_{\alpha\sigma}^{\dagger}(\xi) b_{\alpha\sigma}(\xi - q) \Delta_q + b_{\alpha\sigma}^{\dagger}(\xi) a_{\alpha\sigma}(\xi + q) \Delta_q^* \right\}, \end{aligned} \quad (8)$$

where

$$\Psi_{\alpha\sigma}(x) = \exp(-ip_F x) \sum_{\xi} e^{i\xi x} b_{\alpha\sigma}(\xi) + \exp(ip_F x) \sum_{\xi} e^{i\xi x} a_{\alpha\sigma}(\xi) \quad (9)$$

is a field operator of an electron, with $a_{\alpha\sigma}(\xi)$ and $b_{\alpha\sigma}(\xi)$ being electron annihilation operators near the right and left sheets of the Fermi surface, correspondingly.

Following the same approach as in the theory of superconductivity, we define the normal and anomalous (Gor'kov) Green functions,

$$G_{\alpha\sigma}^{++}(\xi, \tau) = -\langle T_{\tau} a_{\alpha\sigma}(\xi, \tau) a_{\alpha\sigma}^{\dagger}(\xi, 0) \rangle, \quad G_{\alpha\sigma}^{-+}(\xi, \tau) = -\langle T_{\tau} b_{\alpha\sigma}(\xi - q, \tau) a_{\alpha\sigma}^{\dagger}(\xi, 0) \rangle, \quad (10)$$

and derive the corresponding equations of motion,

$$(i\omega_n - [\varepsilon_{\alpha\sigma}^+(\xi) - \mu]) G_{\alpha\sigma}^{++}(\xi, i\omega_n) - \Delta_q G_{\alpha\sigma}^{-+}(\xi, i\omega_n) = 1, \quad (11)$$

$$(i\omega_n - [\varepsilon_{\alpha\sigma}^-(\xi - q) - \mu]) G_{\alpha\sigma}^{-+}(\xi, i\omega_n) - \Delta_q^* G_{\alpha\sigma}^{++}(\xi, i\omega_n) = 0. \quad (12)$$

In this case, the gap is self-consistently determined by

$$\Delta_q^* = -g^2 \sum_{\alpha=1,2} \sum_{\sigma=\pm 1} \sum_{\xi} T \sum_{\omega_n} G_{\alpha\sigma}^{-+}(\xi, i\omega_n), \quad (13)$$

where $\omega_n = 2\pi T(n + 1/2)$ is the Matsubara frequency²⁵.

Solution of a linearized variant of Eqs. (11)-(13) gives us the following transition line between the metallic and CDW phases,

$$\ln\left(\frac{T_{c0}}{T_c}\right) = \frac{1}{4} \sum_{\alpha=1,2} \sum_{\sigma=\pm 1} \sum_{n=0}^{\infty} \frac{v_F^2(q - q_{\alpha\sigma})^2 / (4\pi T_c)^2}{(n + \frac{1}{2})[(n + \frac{1}{2})^2 + v_F^2(q - q_{\alpha\sigma})^2 / (4\pi T_c)^2]}, \quad (14)$$

where $q_{\alpha\sigma}$ are given by Eq. (4). Note that Eq. (14) can be rewritten in a more terse way using the so-called ψ function²⁶,

$$\ln\left(\frac{T_{c0}}{T_c}\right) = \frac{1}{4} \sum_{\alpha=1,2} \sum_{\sigma=\pm 1} \left(\frac{1}{2} \psi\left[\frac{1}{2} + i \frac{v_F(q - q_{\alpha\sigma})}{4\pi T_c}\right] + \frac{1}{2} \psi\left[\frac{1}{2} - i \frac{v_F(q - q_{\alpha\sigma})}{4\pi T_c}\right] - \psi\left[\frac{1}{2}\right] \right). \quad (15)$$

Each of these equations defines the metal-CDW transition line. In particular, they determine a transition temperature T_c for electron spectrum (1) in the presence of a magnetic field using a transition temperature T_{c0} value, corresponding to ideal nesting conditions (i.e., $H = 0$ and $\Delta p = 0$). Note that a competition between the four nesting vectors of Eq. (4), discussed in Sec. II, is directly seen in Eqs. (14), (15).

Numerical solutions of Eq. (14) is presented in Fig. 2, where we use a value of the parameter $\Delta p v_F = 60\text{K}$, determined from a theoretical analysis of the experimentally observed quantum magnetic oscillations¹⁷. As seen from Fig. 2, the Peierls phase is stabilized at high enough magnetic fields, $29\text{T} < H < 49\text{T}$. At very high magnetic fields, $H > 49\text{T}$, and low magnetic fields, $H < 29\text{T}$, an incommensurate CDW phase is shown to be a ground state. We suggest a hypothesis¹⁹ that this incommensurate phase actually corresponds to the SWS ground state. The latter statement is proved by an analysis of the Landau free energy in Sec. IV (see also Fig. 5). We point out that the calculated in this section metal-CDW phase transition line is in very good qualitative and quantitative agreements with the observed one^{13,14}.

IV. FIRST ORDER PHASE TRANSITIONS

It is known that, close to the metal-CDW second order phase transition line, the order parameter is vanishingly small and the Landau theory of the second order phase transitions can be applied. Note that the SWS phase, in the vicinity of the metal-CDW phase transition line, is characterized by the following order parameter,^{21–24}

$$\Delta_{SWS}(x) = \Delta \cos(qx) \cos(2p_F x), \quad (16)$$

which corresponds to mixing of two order parameters (7) with $+q$, Δ_q , and $-q$, Δ_{-q} , where $q \neq 0$. Therefore, below, we derive the Landau free energy up to the fourth order terms in Δ_q and Δ_{-q} and study the mixing of these order parameters in the SWS phase.

A. Free Energy Correction

In this sub-section, we consider the following improved Hamiltonian,

$$\hat{H} = \hat{H}_0 + \hat{H}_I, \quad (17)$$

where \hat{H}_0 is a kinetic energy of free electrons and,

$$\begin{aligned} \hat{H}_I = \sum_{\zeta} \sum_{\alpha\sigma} \{ & \Delta_q a_{\alpha\sigma}^\dagger(\xi + q) b_{\alpha\sigma}(\xi) + \Delta_q^* b_{\alpha\sigma}^\dagger(\xi) a_{\alpha\sigma}(\xi + q) \\ & + \Delta_{-q} a_{\alpha\sigma}^\dagger(\xi - q) b_{\alpha\sigma}(\xi) + \Delta_{-q}^* b_{\alpha\sigma}^\dagger(\xi) a_{\alpha\sigma}(\xi - q) \}, \end{aligned} \quad (18)$$

is a mean-field Hamiltonian for interactions between the electrons and the CDW lattice deformation. In contrast to the Hamiltonian of Sec. III, a possible mixing of the order parameters, Δ_q and Δ_{-q} , has been taken into account in Eq. (18).

Below, we apply to Hamiltonian (18) a diagram technique for a thermodynamic potential, described, for example, in Ref. [25]. This allows us to determine the Landau free energy up to the fourth order terms in the order parameters, Δ_q and Δ_{-q} ,

$$\Delta F = \gamma(|\Delta_q|^2 + |\Delta_{-q}|^2) + \eta_1(|\Delta_q|^4 + |\Delta_{-q}|^4) + \eta_2|\Delta_q\Delta_{-q}|^2, \quad (19)$$

where details of our calculation of the coefficients, γ , η_1 , and η_2 , can be found in Appendix A. [Note that in the paper we consider a so-called incommensurate model of $(\text{Per})_2\text{Pt}(\text{mnt})_2$ electron spectrum. It is an appropriate approximation for our calculations since very weak 1/4 commensurability effects are easily destroyed by small but non-zero corrugations of the Q1D Fermi surfaces in $(\text{Per})_2\text{Pt}(\text{mnt})_2$.]

As known, the coefficient γ determines the metal-CDW transition line if setting to zero. It is positive in the metallic and negative in CDW phases. Therefore, to determine the CDW ground state, we need to minimize the free energy (19) for $\gamma < 0$. In non-SWS phase, where only one order parameter is non-zero (e.g., $\Delta_q \neq 0$ and $\Delta_{-q} = 0$), the minimization procedure results in

$$\Delta F_{NS} = -\frac{\gamma^2}{4\eta_1}. \quad (20)$$

In the SWS phase, where there is a mixing of the order parameters, Δ_q and Δ_{-q} , the free energy is

$$\Delta F_S = -\frac{\gamma^2}{2\eta_1 + \eta_2}. \quad (21)$$

Comparing Eqs. (20), (21), we find the following condition for the appearance of the SWS phase:

$$2\eta_1 > \eta_2. \quad (22)$$

Below, we use Eqs. (20), (21) for the Landau free energy to study the CDW phase in more detail.

B. Results

In this sub-section, the phase transition lines from Peierls phase to the SWS phase are numerically calculated by means of Eqs. (20), (21). We discuss in detail the phase transition lines in the vicinity of $H \approx 49\text{T}$. In the vicinity of $H \approx 29\text{T}$, the phase diagram is qualitatively similar to that in the vicinity of $H \approx 49\text{T}$.

The results of the numerical evaluations of the Landau free energies are shown in Fig. 4, where corrections for both the SWS and non-SWS phases are calculated for the same temperature which is slightly below the metal-CDW transition line. This guarantees a validity of the Landau expansion for the free energies. As seen, at $H < 49.076106\text{T}$, the non-SWS phase has lower free energy, but for higher magnetic fields, the SWS phase is a ground state. Therefore, a true free energy curve has a discontinuity in its slope at the point of a transition from non-SWS to SWS phases, which corresponds to the first order phase transition (see right dashed line in Fig. 5). We also note that at $H = 49.076072\text{T}$, there is a kink in the free energy line, which corresponds to another first-order phase transition. Our detailed numerical calculations show that, between these two first order transitions, there exists a new non-SWS state, which is characterized by an incommensurate nesting vector, $Q \neq 2p_F$.

A detailed phase diagram in the vicinity of $H \approx 49\text{T}$ is shown in Fig. 5. Starting from the Peierls CDW phase, as magnetic field increases, the ground state first becomes a non-SWS CDW state with nontrivial nesting vector, then the system enters into the SWS CDW phase. However, we point out that numerically the region of a stability of the non-SWS incommensurate phase is extremely narrow. Therefore, we expect that thermodynamical fluctuations and hysteresis will result in a direct first order phase transition from the Peierls into SWS phases (see Fig. 2).

V. CONCLUSION

To summarize, we have suggested an explanation of the experimentally observed high resistance state in Q1D organic conductor $(\text{Per})_2\text{Pt}(\text{mnt})_2$. The calculated phase diagram is in good qualitative and quantitative agreements with the existing experiments^{13,14}. We have also predicted the existence of a unique SWS phase, which is characterized by two

energy gaps in its electron spectrum and corresponds to periodically arranged soliton and anti-soliton walls. Our detailed calculations of the Landau free energy demonstrates that there is an incommensurate CDW phase between the commensurate Peierls and SWS phases. Nevertheless, an area of the stability of the incommensurate phase is shown to be numerically extremely narrow, therefore, we suggest that there is a direct first order phase transition from the commensurate Peierls into SWS phases. It is important that the calculated in the paper magnetic field dependence of the Landau free energy of different CDW phases is due to a pure spin contribution. Therefore, the above mentioned first order phase transition can be detected as a divergence of the Knight shift value at the corresponding magnetic field. The SWS phase can be also discovered by a detection of two energy gaps by some infra-red measurements. Indirect confirmation of the existence of the SWS phase in $(\text{Per})_2\text{Pt}(\text{mnt})_2$ is already provided by the measurements of an activation gap¹³, where it is shown that the activation gap becomes very small at low and very high magnetic fields. This fact is in an agreement with the electron energy spectrum of the SWS phase (see Fig.3), which is characterized by two relatively small energy gaps²¹⁻²⁴, although more detailed experimental analysis is needed to make a firm statement. And finally, we suggest neutron and x-rays diffraction experiments in $(\text{Per})_2\text{Pt}(\text{mnt})_2$ to detect the predicted periodic superstructure of soliton and anti-soliton walls directly, which is the main characteristics of the predicted SWS CDW phase.

VI. ACKNOWLEDGEMENT

One of us (A.G.L.) is thankful to N.N. Bagmet, J.S. Brooks, P.M. Chaikin, N. Harrison, M.V. Kartsovnik, and J.S. Singleton for useful discussions. This work was supported by the NSF under Grant DMR-0705986.

APPENDIX: CALCULATION OF γ AND η 's

In this appendix, we give an outline of the calculations of the coefficients γ , η_1 and η_2 appearing in the Landau free energy expansion near the metal-CDW phase transition line (see Eq. (19)).

Feynman diagrams contributing to the second order corrections to the free energy²⁵ with

respect to Δ_q and Δ_{-q} are shown Fig. 6. As a result, we obtain:

$$\gamma = 2\pi \sum_{\alpha\sigma} \sum_{\omega_n} \int \frac{d\xi}{2\pi} G_{\alpha\sigma}^{++}(i\omega_n, \xi + q, H) G_{\alpha\sigma}^{--}(i\omega_n, \xi, H). \quad (\text{A.1})$$

Mathematical technique for evaluation of Eq. (A.1) is standard²⁵, which results in

$$\gamma = -\frac{1}{2v_F T} \sum_{\alpha\sigma} \sum_{n>0} \left\{ \frac{1}{n + \frac{1}{2} + \frac{iv_F(q - q_{\alpha\sigma})}{4\pi T}} + c.c. \right\}. \quad (\text{A.2})$$

In Eq. (A.2), wave vectors $q_{\alpha\sigma}$ are defined by Eq. (4); c.c. stands for a complex conjugate value. After simple calculations, it can be shown that Eq. (A.2) is equivalent to:

$$\gamma = \ln\left(\frac{T_{c0}}{T}\right) - \frac{1}{4} \sum_{\alpha\sigma} \sum_{n=0}^{\infty} \frac{v_F^2(q - q_{\alpha\sigma})^2 / (4\pi T)^2}{(n + \frac{1}{2})[(n + \frac{1}{2})^2 + v_F^2(q - q_{\alpha\sigma})^2 / (4\pi T)^2]}. \quad (\text{A.3})$$

By setting γ to zero, we obtain the metal-CDW second order phase transition line, Eq. (14).

The fourth order terms can be also evaluated by using perturbation theory for a thermodynamic potential²⁵. As it can be shown, $|\Delta_q|^4$ and $|\Delta_{-q}|^4$ terms, corresponding to two diagrams in Fig. 7, have the same coefficients and each such diagram is characterized by a weighting factor 2, therefore,

$$\eta_1 = \frac{1}{32v_F \pi^2 T^5} \sum_{\alpha\sigma} \sum_{n>0} \left\{ \frac{1}{\left[n + \frac{1}{2} + \frac{iv_F(q - q_{\alpha\sigma})}{4\pi T}\right]^3} + c.c. \right\}. \quad (\text{A.4})$$

Two diagrams, corresponding to $|\Delta_q \Delta_{-q}|^2$ term (see Fig. 8), are equal and each of them has a weighting factor 4, therefore,

$$\begin{aligned} \eta_2 = & -\frac{i}{8qv_F^2 \pi T} \sum_{\alpha\sigma} \sum_{n>0} \left\{ \frac{1}{\left[n + \frac{1}{2} + \frac{iv_F(q - q_{\alpha\sigma})}{4\pi T}\right]^2} - \frac{1}{\left[n + \frac{1}{2} - \frac{iv_F(q - q_{\alpha\sigma})}{4\pi T}\right]^2} \right. \\ & \left. - \frac{1}{\left[n + \frac{1}{2} - \frac{iv_F(q + q_{\alpha\sigma})}{4\pi T}\right]^2} + \frac{1}{\left[n + \frac{1}{2} + \frac{iv_F(q + q_{\alpha\sigma})}{4\pi T}\right]^2} \right\}. \end{aligned} \quad (\text{A.5})$$

*Also Landau Institute for Theoretical Physics, 2 Kosygina Street, Moscow, Russia.

-
- [1] W. Dieterich and P. Fulde, Z. Phys. **265**, 239 (1973).
 - [2] L.P. Gor'kov and A.G. Lebed, J. Phys. (Paris) Lett. **45**, L-433 (1984).
 - [3] D. Zanchi, A. Bjelis, and G. Montambaux, Phys. Rev. B **53**, 1240 (1996).

- [4] A.G. Lebed, Pis'ma Zh. Eksp. Teor. Fiz. **78**, 170 (2003) [JETP Lett. **78**, 138 (2003)].
- [5] J.S. Qualls, L. Balicas, J.S. Brooks, N. Harrison, L.K. Montgomery, and M. Tokumoto, Phys. Rev. B **62**, 10008 (2000).
- [6] D. Andres, M.V. Kartsovnik, P.D. Grigoriev, W. Biberacher, and H. Muller, Phys. Rev. B **68**, 201101(R) (2003).
- [7] M. Heritier, G. Montambaux, and P. Lederer, J. Phys. (Paris), Lett. **45**, L-943 (1984).
- [8] A.G. Lebed, Zh. Eksp. Teor. Fiz. **89**, 1034 (1985) [Sov. Phys. JETP **62**, 595 (1985)].
- [9] A.G. Lebed, Phys. Rev. Lett. **88**, 177001 (2002).
- [10] P.M. Chaikin, Mu-Yong Choi, J.F. Kwak, J.S. Brooks, K.P. Martin, M.J. Naughton, E.M. Engler, and R.L. Greene, Phys. Rev. Lett. **51**, 2333 (1983).
- [11] M. Ribault *et al.*, J. Phys. (Paris), Lett. **44**, L-953 (1983).
- [12] *The Physics of Organic Superconductors and Conductors*, edited by A.G. Lebed (Springer, Berlin, 2008).
- [13] D. Graf, E.S. Choi, J.S. Brooks, M. Matos, R.T. Henrique, and M. Almeida, Phys. Rev. Lett. **93**, 076406 (2004).
- [14] J.S. Brooks, D. Graf, E.S. Choi, M. Almeida, J.C. Dias, R.T. Henrique, and M. Matos, J. Low Temp. Phys. **142**, 787 (2006).
- [15] R.D. McDonald, N. Harrison, L. Balicas, K.N. Kim, J. Singleton, and X. Chi, Phys. Rev. Lett. **93**, 076405 (2004).
- [16] E. Canadell, M. Almeida, and J.S. Brooks, Eur. Phys. J. B **42**, R453 (2004).
- [17] D. Graf, J.S. Brooks, E.S. Choi, M. Almeida, R.T. Henriques, J.C. Dias, and S. Uji (unpublished).
- [18] R.D. McDonald, N. Harrison, J. Singleton, A. Bangura, P.A. Goddard, A.P. Ramirez, and X. Chi, Phys. Rev. Lett. **94**, 106404 (2005).
- [19] A.G. Lebed and Si Wu, Phys. Rev. Lett. **99**, 026402 (2007).
- [20] We stress that our model is equivalent to that in Ref.[21] in two limiting cases: at zero magnetic field, $\mu_B H / \Delta p v_F \rightarrow 0$, and at high magnetic fields, $\mu_B H / \Delta p v_F \rightarrow \infty$. Therefore, at high enough and low enough magnetic fields, the SWS phase is characterized by two energy gaps at any temperature in accordance with Ref.[21]. As shown in the paper, the SWS phase is characterized by two energy gaps in the vicinity of the metal-SWS phase transition line for the values of the parameters, $T_c(H = 0) = 7\text{K}$ and $\Delta p v_F = 60\text{K}$. Note that, for higher value

of the parameter Δpv_F , the SWS phase may be characterized by four gaps in its electron spectrum.

- [21] S.A. Brazovskii, I.E. Dzyaloshinskii, and N.N. Kirova, Zh. Eksp. Teor. Fiz. **81**, 2279 (1981)[Sov. Phys. JETP **54**, 1209 (1981)]; M. Fujita, K. Machida, and H. Nakanishi, J. Phys. Soc. Jpn. **54**, 3820 (1985).
- [22] W.P. Su, J.R. Schrieffer, and A.J. Heeger, Phys. Rev. Lett. **42**, 1698 (1979); Phys. Rev. B **22**, 2099 (1980).
- [23] S.A. Brazovskii, S.A. Gordyunin, and N.N. Kirova, Pis'ma Zh. Eksp. Teor. Fiz. **31**, 486 (1980) [JETP Lett. **31**, 456 (1980)].
- [24] S.A. Brazovskii, L.P. Gor'kov, and A.G. Lebed, Zh. Eksp. Teor. Fiz. **83**, 1198 (1982)[Sov. Phys. JETP **56**, 683 (1982)].
- [25] A.A. Abrikosov, L.P. Gorkov, and I.E. Dzyaloshinskii, *Methods of Quantum Field Theory in Statistical Physics* (Dover, New York, 1963).
- [26] I.S. Gradshteyn and I.M. Ryzhik, *Tables of Integrals, Series, and Products* (Academic Press, New York, 1994).

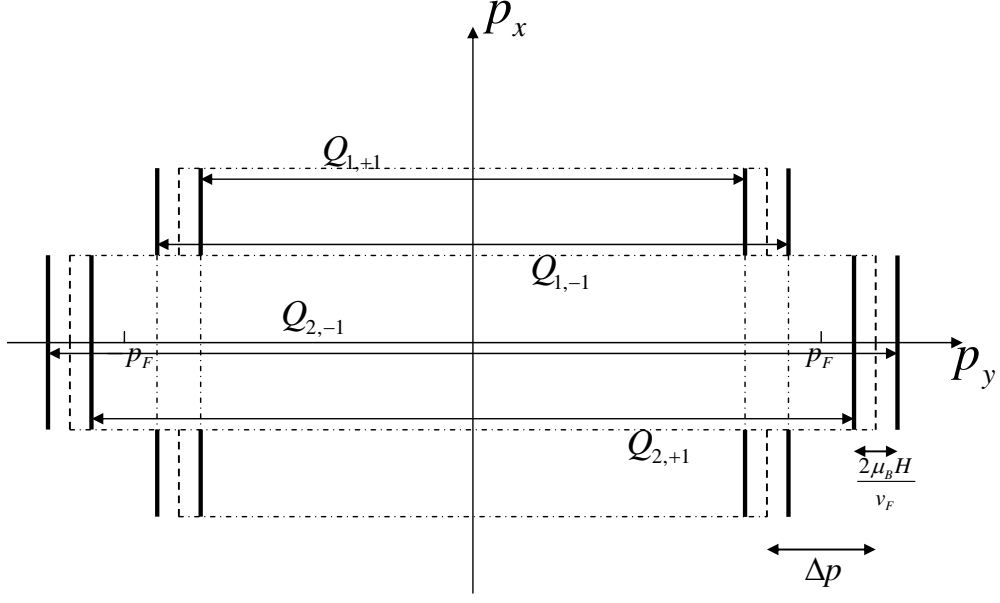


FIG. 1: Fermi surfaces of a Q1D conductor with two conducting chains in a magnetic field. The original four sheets are split into eight ones [see Eq. (2)] and, thus, a competition between the CDW phases is characterized by four different nesting vectors, $Q_{1,+1}, Q_{1,-1}, Q_{2,+1}, Q_{2,-1}$ [see Eqs. (4)]. At magnetic field, $H_p^* = \Delta p v_F / 2\mu_B$, two nesting vectors coincide, $Q_{1,-1} = Q_{2,+1} = 2p_F$, with a half of the original Fermi surface being nested. This results in a restoration of the Peierls CDW phase at high magnetic fields [see Eqs.(5),(14) and Fig.2].

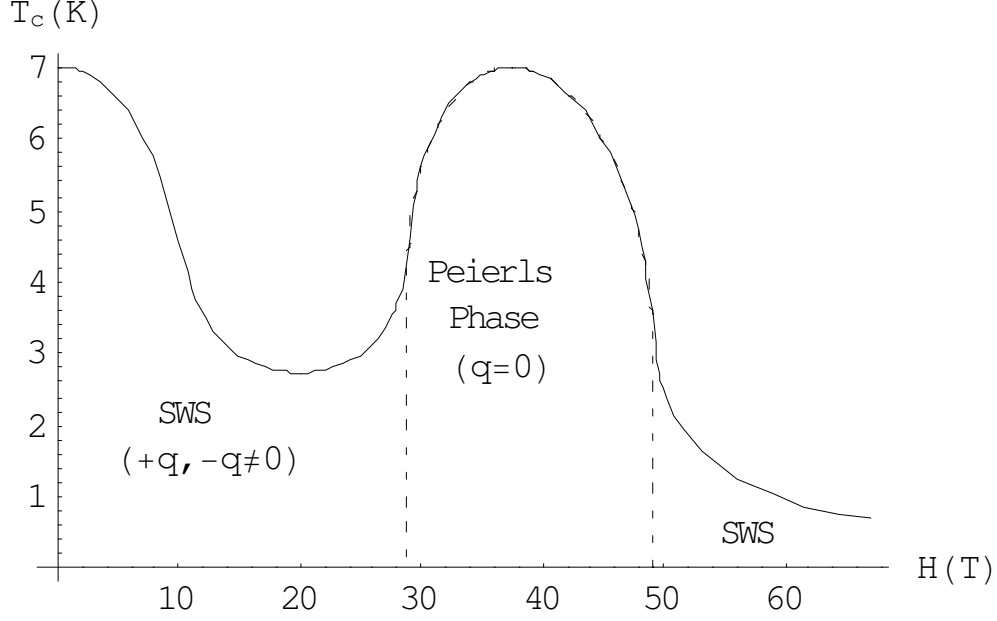


FIG. 2: Hypothetical phase diagram¹⁹ of $(\text{Per})_2\text{Pt}(\text{mnt})_2$ Q1D conductor in a magnetic field. Solid line is a phase transition line between the metallic and CDW phases, calculated from Eq. (14). The dotted lines separate the Peierls and SWS phases. For confirmation of this phase diagram, see Sec. IV and Fig.5.

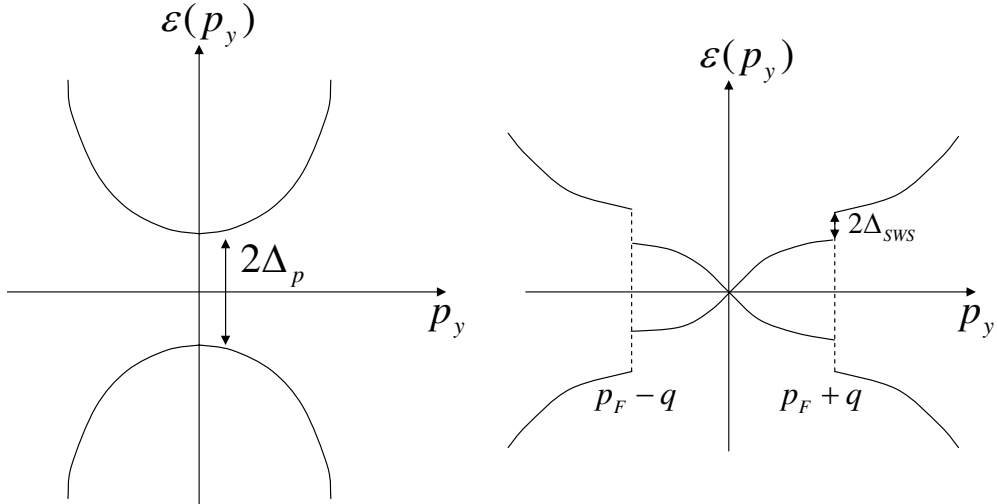


FIG. 3: Electron spectrum of the Peierls phase (left) has one energy gap, Δ_p , whereas the SWS phase (right) is characterized by two smaller energy gaps, Δ_{SWS} . This results in different optical and thermodynamical properties of the Peierls and SWS phases.

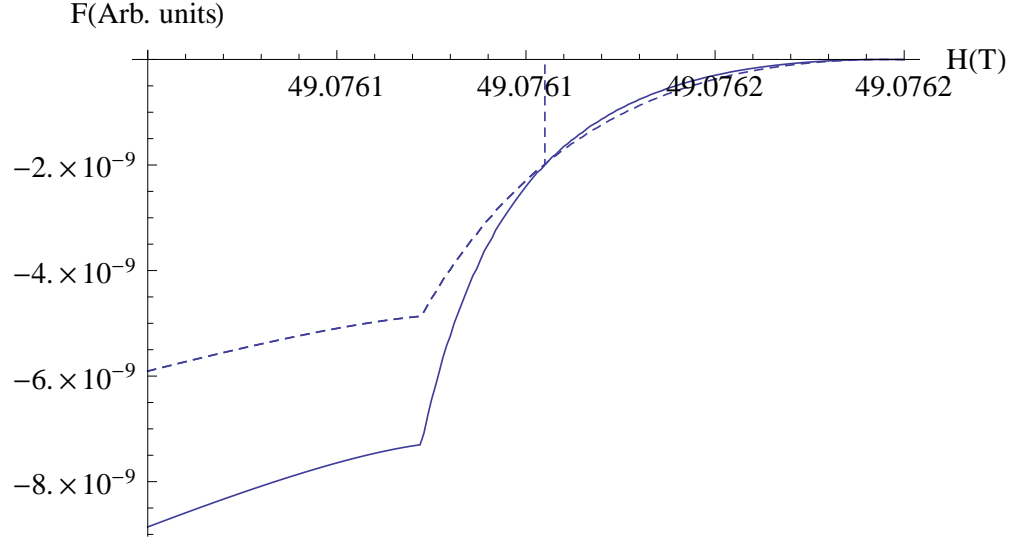


FIG. 4: The Landau free energies (20), (21) in the vicinity of a metal-CDW transition line are calculated in both the SWS and non-SWS phases. Solid and dashed lines stand for the free energies of the non-SWS and SWS phases, respectively.

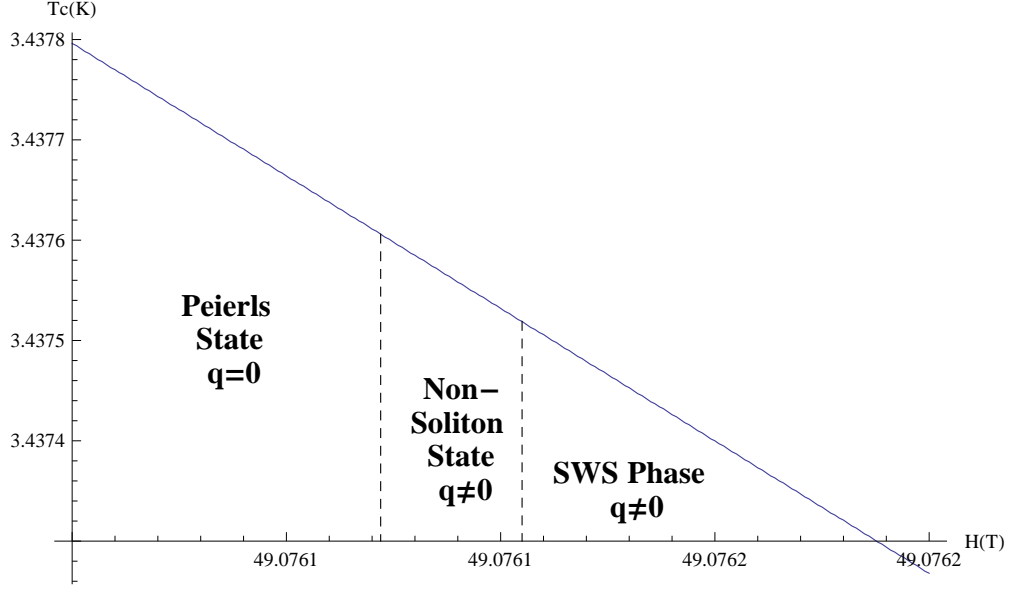


FIG. 5: The detailed phase diagram in the vicinity of $H \approx 49\text{T}$. Solid line: a second order phase transition line between the metallic and CDW phases. Dashed lines: left, the first-order phase transition line from the Peierls state to the incommensurate non-SWS phase with non-trivial nesting vector; right, the first-order phase transition line from the incommensurate non-SWS phase to the SWS phase. Due to extremely narrow region of a stability of the incommensurate non-SDW phase, we expect that there exist a direct first order phase transition from the Peierls to SWS phases.

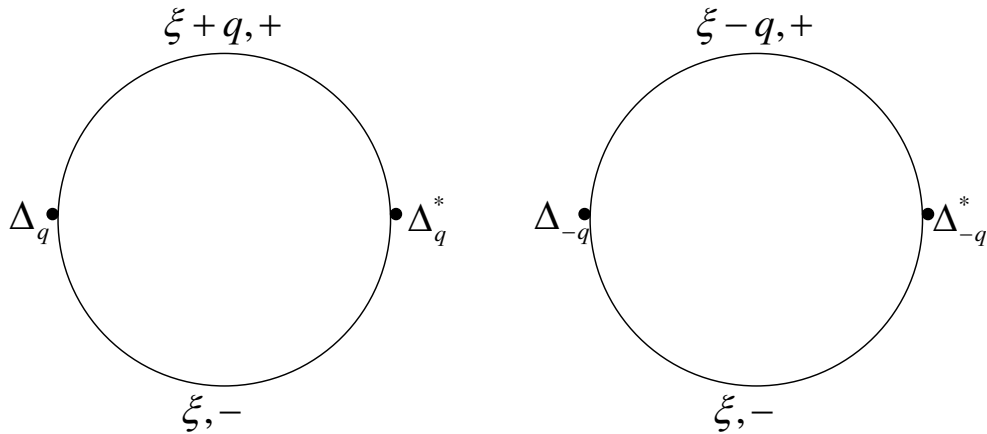


FIG. 6: Second order diagrams, corresponding to the terms, $|\Delta_q|^2$ and $|\Delta_{-q}|^2$, in the Landau free energy (19).

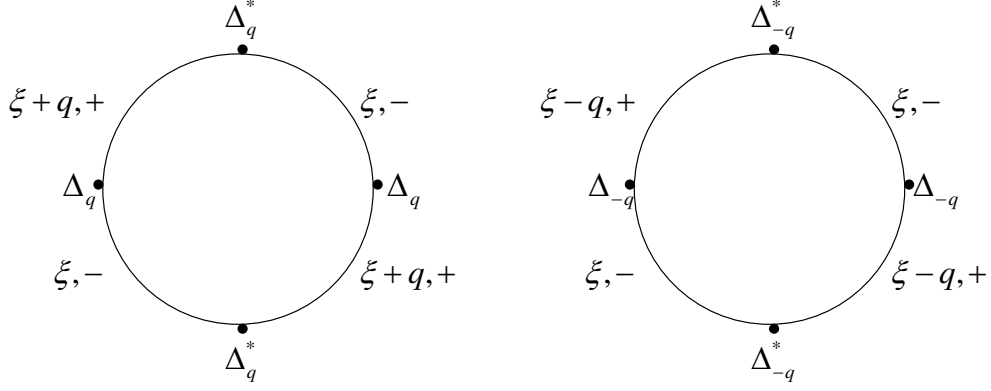


FIG. 7: Fourth order diagrams, corresponding to the terms, $|\Delta_q|^4$ and $|\Delta_{-q}|^4$, in the Landau free energy (19).

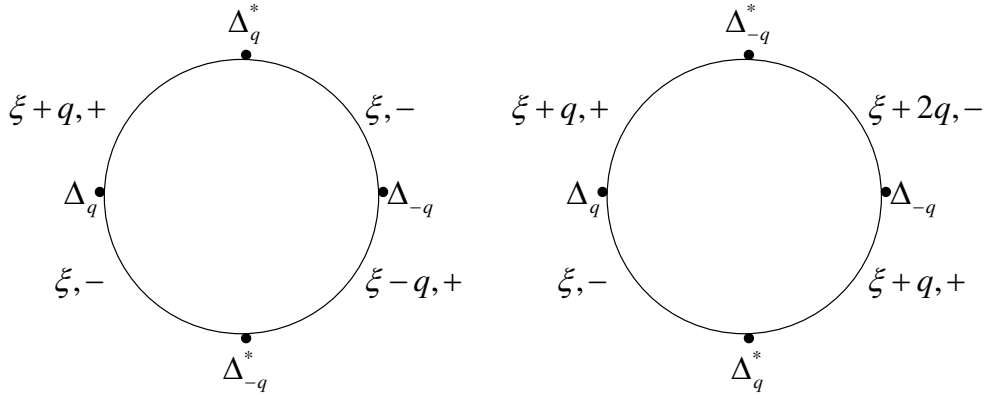


FIG. 8: Fourth order diagrams, corresponding to the term, $|\Delta_q \Delta_{-q}|^2$, in the Landau free energy (19).